Friction

Research Article

Synergistic effects of oleic acid-modified TiO_2 and alkyl polysulfide in forming extreme pressure tribo-films: A mechanistic study

Kai Zeng[1,2], Hongfei Shi[3], Liang Cheng[4], Li Zhang[1], Liang Feng[1], Hengyi Lu[1], Wenjing Hu[1,✉], Jiusheng Li[1,✉]

Cite this article: Zeng K, Shi HF, Cheng L, et al. *Friction* 2026, **14**(3): 9441098. https://doi.org/10.26599/FRICT.2025.9441098

ABSTRACT: The synergistic effect of nanoparticles (NPs) with alkyl polysulfides represents a promising avenue for enhancing extreme pressure (EP) performance in lubricants, potentially reducing the reliance on sulfur-containing additives. However, the underlying synergistic mechanism remains unclear. In this study, oleic acid-modified titanium dioxide (TiO_2-OA) NPs and dialkyl pentasulfide (DPS) formed a mechanically interlocked EP tribo-film with a maximum thickness of approximately 1.4 μm, demonstrating excellent load-bearing capabilities of up to 7,256 N (6.1 GPa). Under conditions of EP friction, the addition of TiO_2-OA NPs facilitates the development of a robust tribo-film of substantial thickness, which in turn bolsters the load-bearing capability of the lubricating oil. Surface analysis of EP wear scars using scanning electron microscopy (SEM), energy dispersive X-ray spectroscopy (EDS), and X-ray photoelectron spectroscopy (XPS) revealed that TiO_2-OA NPs were rapidly deposited and enriched at the friction interface with increasing load (3,530–7,256 N) and friction time (0–10 s), which in turn compensated for the *in situ* wear generated by extreme shear. Cross-sectional analysis of EP wear scars revealed that the preferential formation of ferrous sulfide (FeS) and subsequent rapid enrichment and mechanical interlocking of TiO_2-OA NPs are essential for preventing welding and improving EP performance. This study presents novel insights into the synergistic mechanisms of NPs with sulfur-containing additives, advancing the widespread implementation and progress of NPs in the field of tribology.

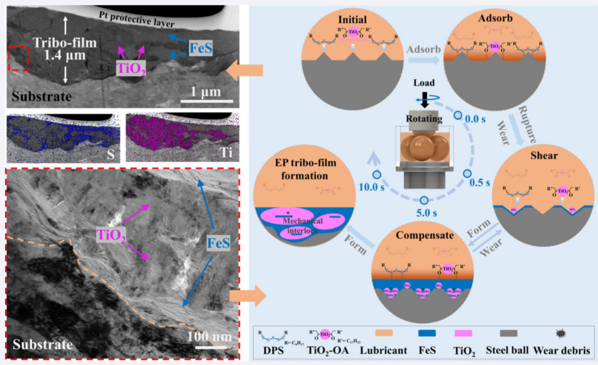

KEYWORDS: TiO_2 nanoparticles; sulfur-containing additives; extreme pressure tribo-film; synergistic mechanism

1 Introduction

Friction and wear inevitably occur and can lead to significant energy dissipation and mechanical component failure [1–5]. In particular, under extreme conditions of severe load, swift motion, and elevated temperature, mechanical components are highly susceptible to lubrication failures that result in severe wear [6–9]. Therefore, to ensure the normal operation of bearings, gears, metal cuttings, hydraulic systems, etc., under extreme conditions, it is necessary to utilize appropriate extreme pressure (EP) lubricants to prevent lubrication failure [5, 10–12]. The EP performance is largely attributable to additives, including zinc dioctyl dithiophosphate (ZDDP), isobutylene sulfide (SIB), dialkyl pentasulfide (DPS), or other sulfur-containing additives. At the friction interface, sulfur-containing additives and the steel friction partner generate a protective ferrous sulfide (FeS) film through a tribochemical reaction [5, 13–15]. This film effectively prevents direct metal-to-metal friction, thereby maintaining lubrication and preventing severe wear and welding [16]. EP performance is dependent on the rapid regeneration of FeS due to its poor mechanical properties and susceptibility to wear under extreme shear [17–19]. This implies that a quantity of sulfur-containing additives must be employed to ensure lubrication under extreme pressure conditions. However, the excessive utilization of sulfur-containing additives has given rise to environmental concerns in recent years [4, 14, 20, 21]. For example, their ecotoxicity represents a threat to the air, water, and soil [14, 22]. Consequently, the utilization of sulfur-containing additives must be decreased while ensuring that the EP performance of the lubricant is not diminished.

Nanoparticles (NPs) have been demonstrated to exhibit superior friction-reduction and anti-wear (AW) characteristics

[1] Laboratory for Advanced Lubricating Materials, Shanghai Advanced Research Institute, Chinese Academy of Sciences, Shanghai 201210, China. [2] University of Chinese Academy of Sciences, Beijing 100049, China. [3] College of Mechanical Engineering, Donghua University, Shanghai 201620, China. [4] College of Chemical Engineering, Guangdong University of Petrochemical Technology, Guangdong 525000, China.

✉ Corresponding authors. E-mail: W. Hu, huwj@sari.ac.cn; J. Li, lijs@sari.ac.cn

Received: October 11, 2024; Revised: February 10, 2025; Accepted: March 18, 2025

[23–29]. Moreover, they can be compounded with sulfur-containing additives to further enhance their EP performance, allowing for a reduction in the amount of lubricant or sulfur-containing additives used. For example, Shen et al. [17] demonstrated that the synergistic effect of SIB with ceria oxide (CeO_2) NPs resulted in a notable enhancement in the AW and EP performance of lubricants. X-ray photoelectron spectroscopy (XPS) analysis of AW wear scars indicated that synergistic effects could be attributed to physisorption, chemisorption, and tribochemical reactions. Similarly, Lei et al. [22] found that the synergistic interaction between CeO_2 NPs and ZDDP promoted both the formation of ultrathick nanocomposite tribo-films (1.17 μm) and improved the maximum seizure-free load (P_B) and load-carrying capacity of the lubricant. The focused ion beam-transmission electron microscopy (FIB-TEM) results indicate that the AW tribo-film is a nanocomposite tribo-film comprising an amorphous phosphate binder and CeO_2 NPs as a filler phase. Guan et al. [30] introduced DPSs into multiwalled carbon nanotubes (MWCNTs). This not only reduced the degree of sliding friction but also resulted in the formation of a protective film at the interface, which reduced the cutting resistance and increased the tool life by 22%. Our previous results demonstrated that the synergistic effect of TiO_2 NPs with SIBs could enhance AW performance, P_B, and the welding load (P_D) [31, 32]. Nevertheless, the mechanism by which TiO_2 NPs enhance EP performance remains unclear. Notably, despite the exceptional EP performance of ZDDP and SIB when utilized independently or in conjunction with other additives, including NPs, existing studies have frequently overlooked comprehensive analyses of EP wear scars, which are pivotal for elucidating the underlying mechanism of EP performance [6, 14, 16, 17, 22, 30–33].

Although the evaluation of AW and EP performance is frequently conducted using a four-ball machine, notable discrepancies exist in the conditions of the two standard tests, as illustrated in Table 1. In fact, EP testing has been observed to elicit more pronounced wear phenomena and generate more distinct friction chemistry than AW testing. For example, under EP conditions, oxygen deficiency occurs at the friction interface, significantly increasing the FeS ratio [34, 35]. Conversely, more sulfate is produced in the AW test [6, 14, 16, 20, 32, 36, 37]. However, few studies have analyzed EP tribo-films containing NPs and sulfur-containing additives. This may explain why the relationship between the composition and formation mechanism of EP tribo-films containing nanoadditives remains unclear. Consequently, it is imperative to explore the relationship between the EP tribo-film structure and EP performance and to understand the synergistic mechanism of NPs and sulfur-containing additives under EP conditions by analyzing EP wear scars.

TiO_2 NPs [29, 38–42] and DPSs [43–45] have attracted considerable research interest because of their superior tribological performance. In this work, the synergistic effect and mechanism of TiO_2-OAs and DPS in 400SN base oil were investigated. The deposition and enrichment of TiO_2 in EP wear scars were found to enhance the shear resistance and hardness of the tribo-film, as evidenced by scanning electron microscopy (SEM), energy dispersive spectrometry (EDS), XPS, and nanoindentation. An EP tribo-film with a maximum thickness of approximately 1.4 μm was observed in the EP wear scars using FIB-TEM. Furthermore, FeS was preferentially formed, followed by mechanical interlocking and nonuniform mixing of TiO_2-OA with FeS, which resulted in the creation of micrometer-scale tribo-films. This observation provides direct support for the understanding of the synergistic mechanism of TiO_2-OA and DPS, as well as the EP tribo-film formation process.

Table 1 Comparison of AW and EP test standards

Test type	Load (N)	Friction time	Temperature (°C)
AW test [46]	147–392	30–60 min	75
EP test [47]	784 or more	10 s	18–35

2 Experimental

2.1 Materials

Tetrabutyl titanate (TBT; 99%) and oleic acid (OA; 90%+) were obtained from Shanghai Titan Scientific Co., Ltd., China. 400SN mineral oil was supplied by Dalian Petrochemical Corporation (Table S1 in the Electronic Supplementary Material (ESM)). Dialkyl pentasulfide (DPS) was purchased from Shanghai Starry Chemical Co., Ltd., China. All reagents were used without additional purification, and the water used was deionized (DI) water.

2.2 Sample preparation

As shown in Fig. 1(a), the sol–gel method was used to prepare oleic acid-modified TiO_2 (TiO_2-OA) NPs [28]. Specifically, a mixture of 50.0 g TBT (147 mmol) and 41.5 g OA (147 mmol) was prepared, which was then heated to 60 °C and vigorously stirred for 1 h. Subsequently, 5.3 g of DI water was added dropwise, the temperature was maintained at 60 °C, and the mixture was vigorously stirred for 6 h. Finally, the viscous oleic acid-modified TiO_2 (TiO_2-OA) is obtained by vacuum distillation to remove water and n-butanol. TiO_2-OA NPs with molar ratios of 1:0.5, 1:1, 1:1.5, 1:2, and 1:3 were synthesized by maintaining a constant amount of TBT while varying the quantity of oleic acid. Test sample oils were obtained by adding TiO_2-OA (0–3.0 wt%) and DPS (0–4.0 wt%) to 400SN followed by mechanical stirring and ultrasonication. TiO_2-OA, DPS, and the combination of TiO_2-OA and DPS were added to the 400SN, which were denoted as 400SN+TiO_2-OA, 400SN+DPS, and 400SN+DPS+TiO_2-OA, respectively.

2.3 Tribological tests

The friction-reduction, EP and AW performances of the lubricants were tested using a four-ball tribometer (Xiamen Tianji Automation Co., Ltd.). GCr15 steel balls with a diameter of 12.7 mm, an elastic modulus of 210 GPa, and a Poisson's ratio of 0.30 were used as the friction pair for the above tests. The P_D and P_B values, which serve as crucial indicators of EP performance, are measured in accordance with the standard methods ASTM D2783-21 (Table 1) and GB/T 12583-98 (ASTM D2783-98), respectively. Furthermore, minor adjustments were made to the standard method to ascertain more accurate welding loads. Specifically, to guarantee the dependability and reproducibility of the experimental outcomes, the load was incremented by 196 N at each stage until the desired welding load was attained. Friction reduction and AW performance were evaluated by comparing the coefficient of friction (COF) and wear scar diameter (WSD) under conditions of friction at 196 N, 1,200 r/min, and 75 °C for 60 min, respectively. WSD was quantified using optical microscopy, and the COF was continuously monitored by a four-ball tribometer. Each test was conducted in triplicate, and the repeatability was performed in accordance with the standard method. The tribological performance and load-carrying capacity of the lubricant were also evaluated on a ball-plate reciprocating friction

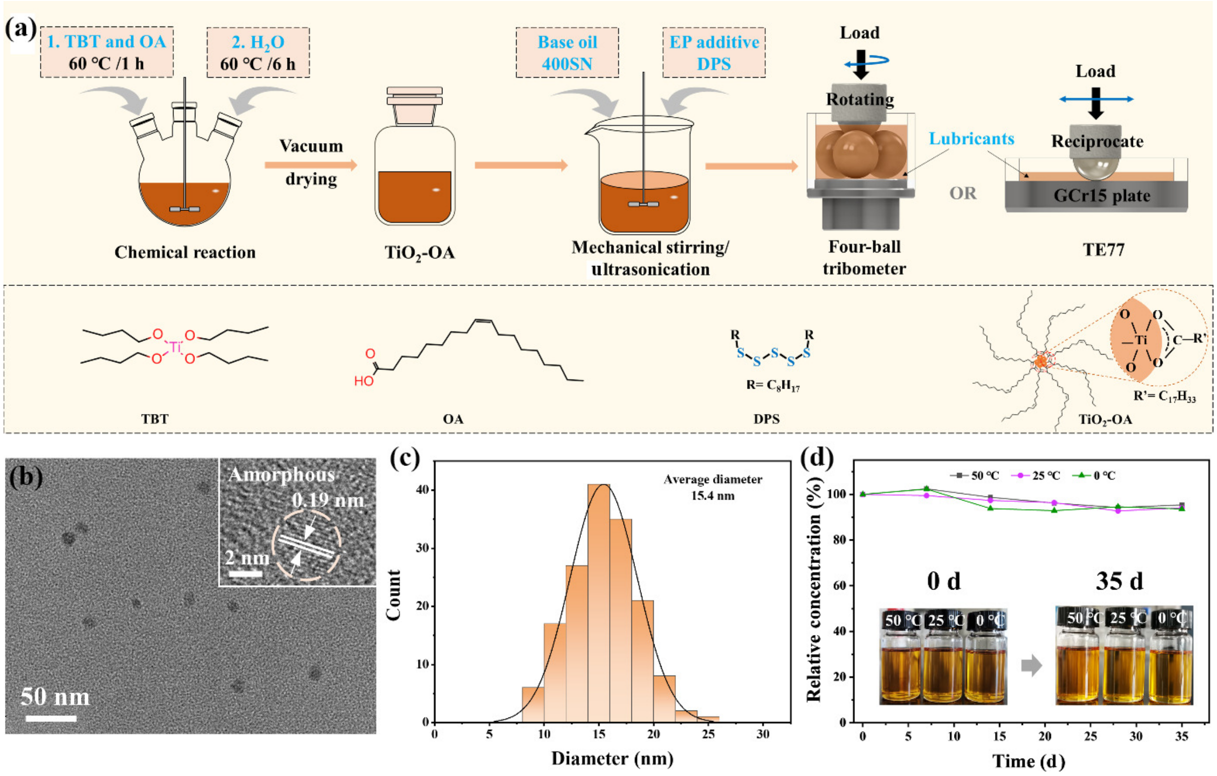

Fig. 1 Preparation and characterization of TiO_2-OA NPs. (a) Schematic of preparation and application of TiO_2-OA. (b) TEM and HRTEM images (inset). (c) Particle size distribution image. (d) Relative concentration curve of TiO_2-OA in lubricant and photographs of dispersion stability (inset).

machine (TE77). The balls and plates are made of GCr15 bearing steel. The friction parameters were as follows: 250 N, 50 °C, 20 Hz, and 60 min. In a four-ball tribometer or TE77, the top ball rotates or reciprocates, whereas the lower three balls or plates remain stationary. All tribopairs were ultrasonically cleaned with petroleum ether both before and after the analysis.

2.4 Material characterization

The structural characteristics and particle size distributions of the TiO_2-OA NPs were observed using a transmission electron microscope (TEM; 2100F, JEOL). The crystal structure data of TiO_2-OA were obtained with a Bruker X-ray diffractometer (XRD; D8 Advance). The dispersion stability of TiO_2-OA in 400SN was evaluated by optical microscopy and ultraviolet–visible spectroscopy, employing the Lambert–Beer law. The thermal stability of TiO_2-OA under nitrogen conditions was evaluated using a thermogravimetric analyzer (TGA; TGA55, TA). The water contact angle of the steel plate after lubricant wetting was measured using the seated drop method. Specifically, the cleaned steel plates were immersed in lubricating oil for 1 h, gently rinsed with toluene, dried with nitrogen, and then subjected to water contact angle measurements. The FT-IR spectra of the samples were acquired using an FT-IR spectrometer (Spectrum Two, PerkinElmer). The particle size distribution and zeta potential of the sample (dispersed in base oil at approximately 0.1 wt%) were measured at 25 °C using dynamic light scattering (DLS) and electrophoretic light scattering (ELS) with a Zetasizer Nano ZS90 (Malvern). The chemical structure and composition of the samples were determined by an X-ray photoelectron spectroscope (ESCALAB 250xi, Thermo). The surface morphology of the wear scars on the steel balls was examined by a field emission scanning electron microscope (GeminiSEM 300, Zeiss), and the types and distributions of the elements in the friction zone were analyzed by EDS. The wear surfaces and trajectories were investigated using two-dimensional images acquired by a white-light interferometer (WLI; ContourGT-K, Bruker), along with the corresponding cross-sectional profile images. Nanoindentation tests were performed on a nanoindenter (NanoTest Vantage, MML, MechAction). A focused ion beam (FIB; Helios NanoLab 600i, FEI) system was employed to extract the cross-sectional profile of the tribo-film situated in the center of the steel ball wear trace. To ensure the structural integrity of the wear surface, a platinum (Pt) protective layer was applied to the surface of the wear point prior to the use of the FIB system. The microstructure of the tribo-film was investigated using a transmission electron microscope (Titan Cubed Themis G2300, FEI).

3 Results and discussion

3.1 Characterization of TiO_2-OA NPs

Ultrafine oil-soluble TiO_2-OA NPs were prepared using the sol–gel method (Fig. 1(a)). As shown in the TEM image (Fig. 1(b)) and particle size distribution (Fig. 1(c)), the prepared TiO_2-OA NPs exhibited no discernible agglomeration phenomenon, with an average particle size of 15.4 nm. This conclusion is corroborated by the results of dynamic light scattering (Fig. S1(a) in the ESM). A limited number of lattice fringes were discernible in the high-resolution transmission electron microscopy (HRTEM) image (Fig. 1(b)). The presence of TiO_2 nanocrystals, which are surrounded by amorphous TiO_2, was observed in only a limited region of the TiO_2-OA sample. The lattice spacing of 0.19 nm corresponds to the (200) crystal plane of anatase TiO_2 [48, 49]. Nevertheless, lattice fringes are not observed in the majority of regions and show an amorphous structure, which is consistent with the XRD results (Figs. S1(b) and S1(c) in the ESM). This outcome is in accordance with previous studies in Refs. [49–51]. The FT-IR spectra, XPS spectra, TGA curves, and zeta potential clearly demonstrate that the TiO_2 surface was successfully modified with OA, conferring oil-soluble performance and stability (Fig. S1 in the ESM and Fig. 1(d)). The dispersion stability of TiO_2-OA in 400SN is satisfactory, despite its relatively low absolute zeta potential. This suggests that the dispersion stability may be attributed primarily to steric or electrosteric stabilization rather than solely electrostatic stabilization [52, 53]. These results are consistent with our previous studies and indicate the potential of TiO_2-OA as a lubricant additive [31, 32]. Moreover, the addition of TiO_2-OA and DPS did not significantly alter the water contact angle of the steel plate after lubricant wetting or the kinematic viscosity of the base oils (Fig. S2 in the ESM).

3.2 Extreme pressure performance of TiO_2-OA and DPS

The P_B and P_D values represent key indicators of the EP performance of a lubricant and are employed to assess the potential of that lubricant to form an EP tribo-film under extreme conditions [17, 22, 54]. As illustrated in Fig. 2(a), the wear scar diameter (WSD) increases with increasing load, particularly after the load exceeds the critical value (P_B value), where a notable increase in WSD is observed. This is due to the boundary film being broken down when the load exceeds the P_B value, causing a notable increase in wear [17]. The regions below and above the P_B value are typically defined as the AW and EP regions, respectively. The addition of TiO_2-OA not only serves to reduce the WSD of both 400SN and 400SN+DPS but also broadens the EP region. This suggests that a strong chemical tribo-film is formed at the friction interface, resulting in favorable EP performance. As illustrated in Figs. 2(b) and 2(c), the lubricants exhibited different EP performances. The addition of TiO_2-OA led to an increase in both the P_B and P_D values of 400SN and 400SN+DPS. In particular, TiO_2-OA can increase the P_D value of 400SN+DPS by 29% (Fig. 2(c)). Although the P_D values with 400SN+TiO_2-OA were not as favorable as those observed with 400SN+DPS, the addition of TiO_2 did increase the P_D values of 400SN (Fig. 2(c)), a result that is similar to those of previous studies [27, 28]. Furthermore, continuously increasing load experiments in reciprocating mode were conducted at TE77 to evaluate the load-bearing capability of lubricants. As illustrated in Fig. S3 in the ESM, 400SN+DPS+TiO_2-OA exhibited superior load-bearing capacity and tribological behavior compared with either DPS or TiO_2-OA alone. This finding is consistent with the data presented in Figs. 2(b) and 2(c). Compared with 400SN+DPS, 400SN+DPS+TiO_2-OA notably increased the P_D value and load-bearing capacity, which suggests that TiO_2 NPs and DPS synergize to form a stronger tribo-film. Unexpectedly, the contact potential of 400SN+TiO_2-OA increased significantly during friction, but the contact potentials of 400SN+DPS and 400SN+DPS+TiO_2-OA did not increase (Fig. S3(b) in the ESM). This may be due to the difference in electrical conductivity between TiO_2 and iron sulfides [55, 56]. TE77 utilizes a Lunn–Furey electrical contact resistance circuit, whereby an increased contact potential indicates increased resistance within the contact area, which might be associated with the development of a tribo-film. This phenomenon was also observed by Wu et al. [57].

A modification of the standard method (ASTM D2783) has been utilized to determine more accurate welding loads and to investigate the synergistic mechanism of TiO_2-OA and DPS. Specifically, the load was increased gradually to 196 N/test before the weld load (modified P_D) was reached. As illustrated in Fig. 2(d), the modified P_D is positively correlated with the DPS content. Moreover, TiO_2-OA has the potential to enhance the modified P_D at varying contents of DPS, with the effect being particularly pronounced above 3%, which can be increased by approximately 21%. Importantly, the DPS content of 2.5% is deemed to lack an enhancement effect on the P_D value.

Following the confirmation of the synergistic effect of TiO_2-OA and DPS, further studies were conducted to clarify the effects of TiO_2 NPs on the EP performance of lubricants. This involved examining the ratio of the surface modifier OA to TBT and the impact of the TiO_2-OA content on the modified P_D value. The evidence in Fig. 2(e) suggests that an increase in the molar ratio of OA may result in a reduction in the modified P_D value. According

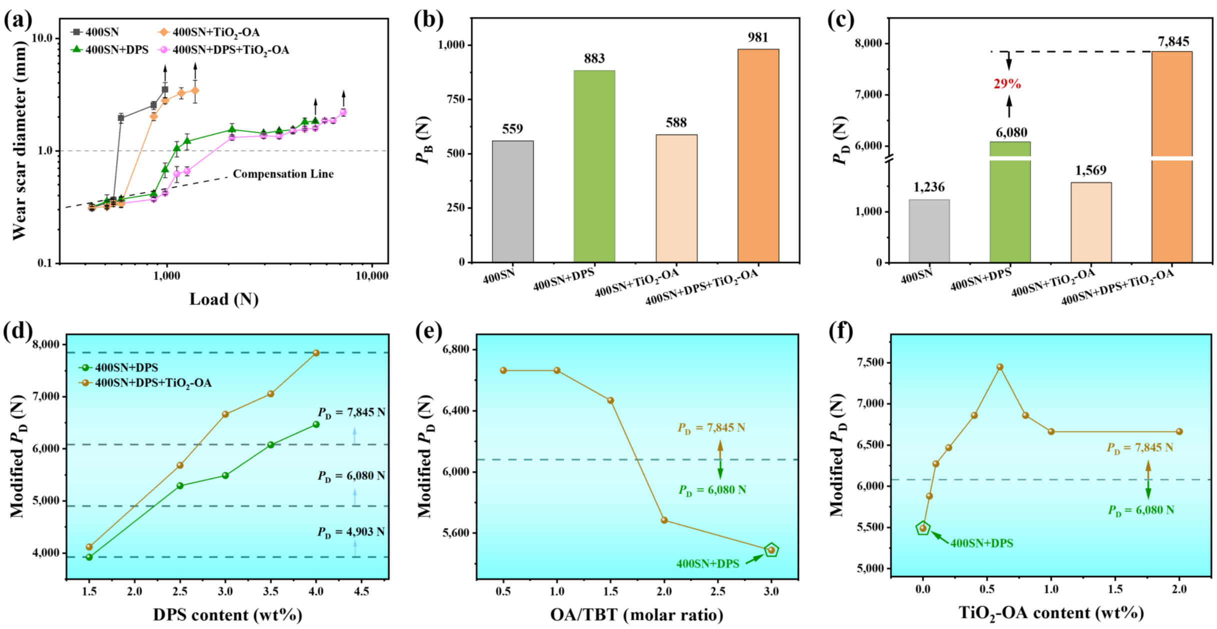

Fig. 2 EP performance of 400SN base oils and oils containing DPS and TiO_2-OA (four-ball tribometer). (a) Wear scar diameter versus load. (b) P_B values and (c) P_D values according to standard method (3% DPS+1% TiO_2-OA). (d) Modified P_D values for different DPS contents (1% TiO_2-OA), (e) modified P_D values for different OA and TBT molar ratios (3% DPS+1% TiO_2-OA), and (f) modified P_D values for different TiO_2-OA contents (3% DPS) according to adjusted ASTM D2783 (196 N or 20 kgf per grade). Standard grade is around dotted line.

to the standard method, an OA:TBT mole ratio of 0.5–1.5 is associated with an enhancement effect. However, this is not the case when the ratio is equal to 2.0. Notably, when the OA:TBT ratio reached 3, the modified P_D values of 400SN+DPS+TiO_2-OA were identical to those of 400SN+DPS, indicating the absence of a synergistic effect. Figure 2(f) shows that the modified P_D value initially increases and subsequently decreases with increasing TiO_2-OA content. Its optimal content is 0.6%, with a modified P_D value of 7,453 N, which is an enhancement of approximately 36% relative to 400SN+DPS. Further studies have shown that the addition of additional OA to 400SN+DPS leads to a definitive decrease in the modified P_D value (Fig. S4 in the ESM). These results exclude the possibility that excess OA in TiO_2-OA enhances the P_D value, further corroborating the contribution of TiO_2-OA to the synergistic effect. Furthermore, the addition of only 0.1 wt% TiO_2-OA increased the P_D from 6,080 to 7,845 N (29% improvement) when the DPS content was 3% in accordance with the standard method (Fig. 2(f)).

3.3 Surface characterization of EP wear scars on preweld balls

The additives in lubricants have the potential to produce chemical tribo-films at the contact surface through three mechanisms: adsorption, chemical reactions, and deposition [1]. Figure 3 illustrates the chemical tribo-film and synergistic mechanism of DPS and TiO_2-OA under EP conditions on the wear scars following 10 s of friction at loads ranging from 3,530 to 7,256 N. SEM images (Fig. 3(a)) reveal that deep grooves are present in both lubricants in the sliding direction. However, there is a notable difference in the distribution of these grooves. The deep grooves of 400SN+DPS are distributed on the two sides of the wear traces, whereas those of 400SN+DPS+TiO_2-OA are concentrated on the upper side of the sliding direction. EDS maps (Fig. 3(b)) reveal that regions without deep grooves in the 400SN+DPS+TiO_2-OA lubricated wear scars exhibit an enrichment of Ti and O elements, with nearly overlapping distributions. Notably, the appearance of deep grooves is not indicative of weakness in the Ti-containing tribo-film with respect to shear in the 400SN+DPS+TiO_2-OA lubricated wear scars. Conversely, this may indicate that the Ti-containing tribo-film is highly resistant to extreme shear. The percentage of Ti increases with increasing applied load in the central region of the wear scars (Fig. 3(b) and Table 2), and the relative content of Ti increases with increasing rubbing period in the central region of the wear scars (Figs. S5 and S6 in the ESM). As shown in Fig. 3(b), the distribution of S is relatively uniform, with no large blank areas. This finding indicates that the coverage of the tribo-film is generally uniform. Concurrently, the tribo-film maintains its protective effect under a load of 7,256 N, which indicates that its adhesion strength remains robust. As might be expected, the WSD exceeds 1 mm within 0.5 s under EP conditions, thus supporting the view that boundary film failure causes a surge in wear (Table S2 in the ESM). Further observation revealed that the lubricant 400SN+DPS produced a finer tribo-film with exfoliation, whereas the lubricant 400SN+DPS+TiO_2-OA was able to form a denser tribo-film (Fig. S7 in the ESM). Additionally, the nanoindentation results demonstrated that the hardness of the tribo-film formed by 400SN+DPS+TiO_2-OA was greater (Fig. S8 and Table S3 in the ESM). The results indicate that the chemical

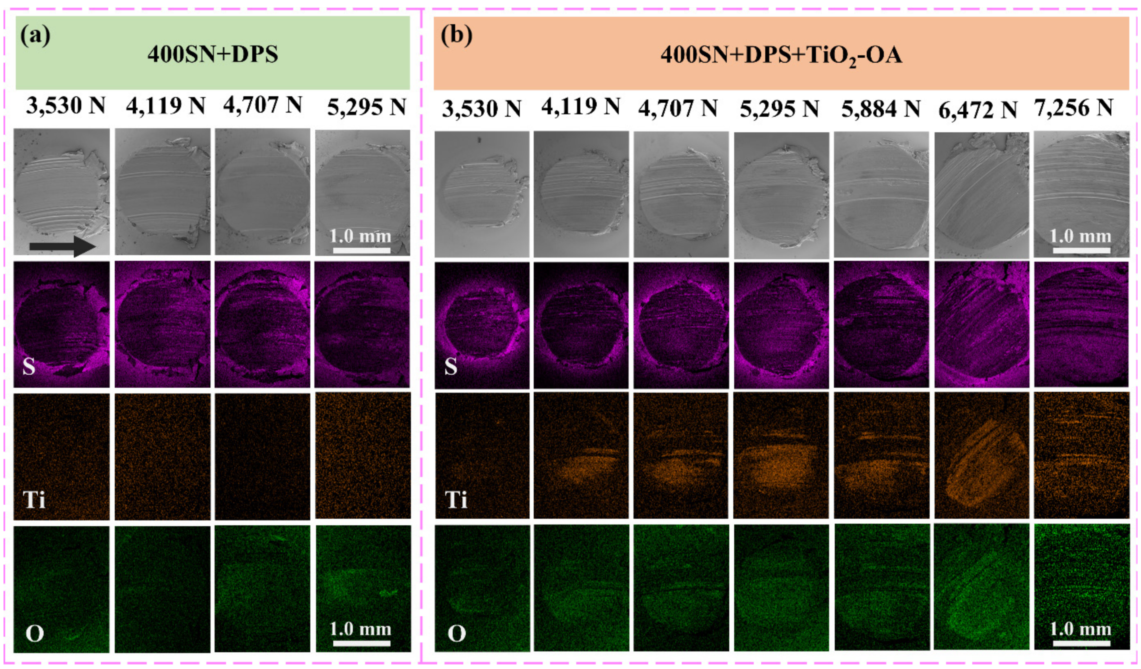

Fig. 3 SEM images and EDS maps of EP wear scars (3% DPS+0.6% TiO_2-OA; arrow shows direction of sliding).

Table 2 Percentage elemental content of wear scar surface (XPS)

Sample	Load (N)	Element percentage content (%)				
		C 1s	O 1s	Fe 2p	S 2p	Ti 2p
400SN+DPS	5,295	56.2	30.5	6.6	6.6	0.0
400SN+DPS+TiO_2-OA	5,295	59.2	26.7	6.6	6.5	1.0
400SN+DPS+TiO_2-OA	6,472	60.4	27.2	5.6	4.9	1.9

tribo-film formed by 400SN+DPS+TiO_2-OA is more resistant to cutting and high temperatures and has a higher load-bearing capacity than the tribo-film formed by 400SN+DPS. This finding provides evidence that TiO_2-OA can compensate for the EP tribo-film and increase the P_D value.

To gain further insight into the relationships among the constitutive elements and state of the tribo-film, XPS spectra of the EP wear scars of 400SN+DPS and 400SN+DPS+TiO_2-OA are presented in Fig. 4. The signals observed at 161.4, 162.7, and 164.0 eV in the S 2p spectrum indicate the presence of a metal sulfide (FeS) and thiols, respectively (Fig. 4(b)) [6, 16, 17, 36]. The signal at ~169 eV in the S 2p spectrum is believed to originate from metal sulfate ($FeSO_4$/$Fe_2(SO_4)_3$), a result of further oxidation of sulfide in the AW test [6, 14, 16, 20, 32, 36, 37]. However, no evidence of metal sulfates was observed on the wear scars, while the characteristic peaks of the metal sulfides were quite distinct. This indicates that FeS becomes the predominant form of S present in the tribo-film in the EP test, and there is no formation of metal sulfate. The cause of this event may be associated with the brief duration of the EP test and the insufficient supply of oxygen at the friction interface, which resulted in the lack of further oxidation of FeS to metal sulfates [34, 35]. As illustrated in Fig. 4(c), the characteristic peak of C 1s at 284.8 eV is indicative of the C–C bond [22]. The presence of Ti $2p_{3/2}$ (458.5 eV) and Ti $2p_{1/2}$ (464.5 eV) on the wear scars of 400SN+DPS+TiO_2-OA lubrication can be attributed to the adsorption and deposition of TiO_2 at the contact surface (Fig. 4(d)) [58]. As illustrated in Fig. 4(e), the O 1s spectra of all three wear scars exhibit signal peaks at 532.2, 531.4, and 530.0 eV, which are attributed to C–O bonds, C=O bonds, and metal oxides, respectively [59, 60]. Nevertheless, the metal oxide signal peaks are more pronounced in 400SN+DPS+TiO_2-OA than in 400SN+DPS. It is conceivable that the presence of TiO_2 within the tribo-film may have resulted in the observation of relatively strong metal oxide signals in the O 1s spectrum of 400SN+DPS+TiO_2-OA. The characteristic peak present at 707.4 eV in the Fe 2p spectrum indicates the presence of FeS (Fig. 4(f)) [16, 17]. The signals observed at 710.5 and 712.5 eV in the Fe 2p spectrum are indicative of the presence of FeO, Fe_3O_4, Fe_2O_3, and/or FeOOH, respectively [22, 61, 62]. These oxidized iron species are produced primarily by chemical reactions between Fe and O_2 at the friction interface. The results show that the EP test resulted in stronger FeS and metal oxide signals on the wear scars, indicating significant differences in friction chemistry and tribo-film compared with the AW test [34, 35].

3.4 Cross-sectional analysis of EP tribo-films on preweld balls

To explore the microstructure of the tribo-film produced under EP conditions, a FIB system was used to obtain cross-sectional samples of wear scars on the surface of steel balls lubricated with 400SN+DPS+TiO_2-OA. Figures 5(a) and 5(b1) demonstrate the presence of a tribo-film of varying thickness between the Pt protective layer and the substrate (steel ball). The tribo-film thickness ranges from 0.6 to 1.4 μm, which significantly exceeds the approximately 0.1 μm thickness of the tribo-film produced by ZDDP [22]. This increased thickness is attributed to the aggregation of TiO_2 NPs. Notably, the sintering load of steel balls under EP conditions is significantly influenced by the cutting resistance and regeneration rate of the tribo-film [18]. The TEM images and EDS maps (Figs. 5(b1)–5(b5) and 5(c1)–5(c5)) demonstrate that the elements Fe and S significantly overlap, whereas the regions enriched with Ti and O are nearly identical. The EDS maps indicate that the light and dark areas in Figs. 5(b1) and 5(c1) correspond to enriched regions of FeS and TiO_2, respectively. The elemental content (Table S4 in the ESM) indicates that the TiO_2-enriched region in the tribo-film contains a significantly lower amount of carbon than titanium does. This phenomenon may be attributed to the high temperature generated by friction under EP conditions. The high temperature causes the breakage of the TiO_2-OA ester bond, leading to the aggregation of TiO_2 NPs into larger clusters. The tribo-film is clearly a nonuniformly mixed composite layer comprising FeS and TiO_2, which differs from the AW tribo-film reported by Lei et al. [22]. CeO_2 NPs were observed to be distributed uniformly in the AW tribo-film, which was produced by the synergistic action of ZDDP and CeO_2 [22]. Furthermore, it has been demonstrated that nanodiamonds (NDs) are uniformly distributed within the

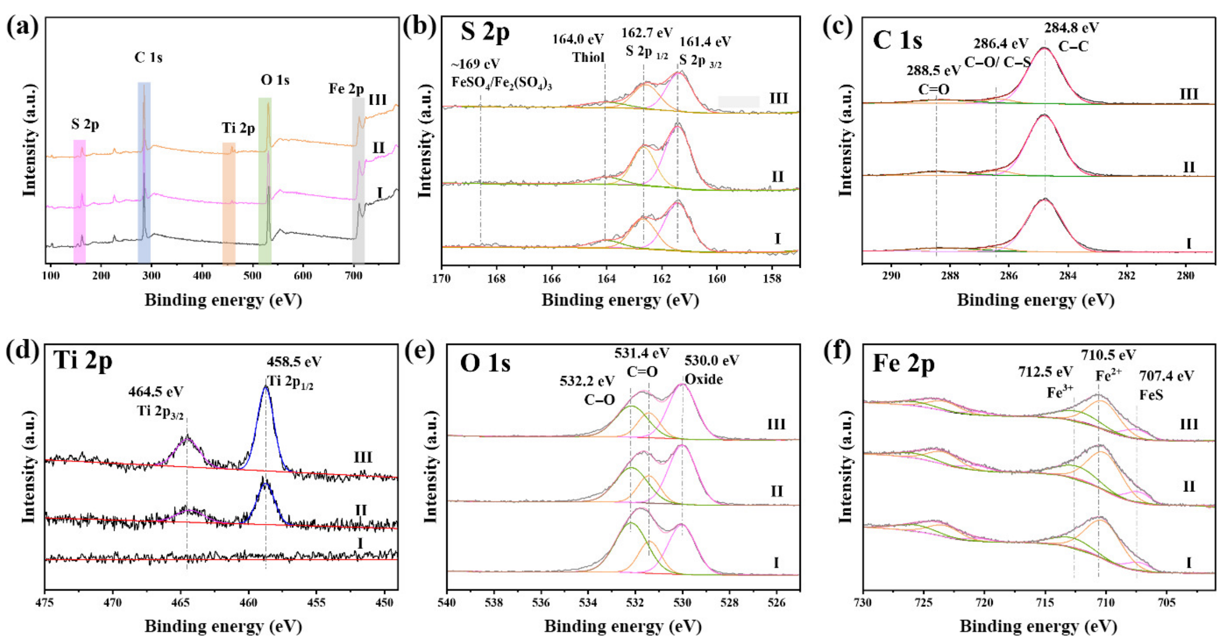

Fig. 4 XPS analysis of AW wear scar surface elements (I: 400SN+DPS_5,295 N, II: 400SN+DPS+TiO_2-OA_5,295 N, III: 400SN+DPS+TiO_2-OA_6,472 N).

ZDDP tribo-film, which results in mechanical interlocking and enhances the retention of the tribo-film, thereby reducing the COF [63]. This observation suggests a structural disparity between the EP and AW tribo-films. Figures 5(c1)–5(c5) demonstrate that the filamentous region of the tribo-film is principally composed of FeS, whereas the dense portion is primarily TiO_2. The HRTEM findings reveal the presence of nanograins within the amorphous phase (Fig. 5(d)). The measured lattice spacing of 0.26 nm can be attributed to the FeS (101) crystal plane [64–66]. The contact area of the tribo-film with the substrate in Fig. 5(e) reveals that FeS is located closest to the substrate and is approximately 50 nm thick. TiO_2 and FeS then follow closely. This suggests that the DPS preferentially reacts with the steel ball, whereas TiO_2 and FeS swiftly compensate for and fill in defects, ultimately forming a mechanically interlocked EP tribo-film.

The thickness of the tribo-film is subject to various influencing factors, including the type of friction sub, the base oil, and the additives, in addition to external conditions such as load, friction time, and contact pressure. Figure 5(f) presents the statistical data regarding the maximal thickness of the tribo-film extracted using FIB. The maximal thickness of the tribo-film for the combination of ZDDP and NPs is significantly greater than that of ZDDP or NPs alone at varying contact pressures. However, both tribo-films were obtained under low load or low contact pressure conditions rather than under EP conditions. In this work, the EP tribo-film thickness was observed to range from 0.6 to 1.4 μm under an ultrahigh load of 7,256 N (initial contact pressure of 6.1 GPa) and a friction time of 10 s. Considering the severe wear that occurs during EP testing, a thicker tribo-film may offer advantages in enhancing EP performance (P_D value). However, this does not imply that the maximum tribo-film thickness can be used as a very suitable indicator. Future research should focus on the thickness range, average thickness, coverage, and adhesion strength of the tribo-film and conduct more in-depth analysis.

It has been demonstrated that FeS has weaker mechanical properties than steel does and is readily sheared [17, 78]. Moreover, the melting point of FeS (1,193 °C) is much lower than that of TiO_2 (1,854 °C) [79–81]. It can be assumed that the tribo-film composed of TiO_2 and FeS is capable of withstanding higher shear and higher temperature than the FeS tribo-film. The growth of the EP tribo-film seems to be the direct cause of TiO_2-OA enhancing the P_D value of 400SN+DPS. This provides further evidence that the combined use of sulfur-containing additives and NPs can result in enhanced EP performance of the lubricant.

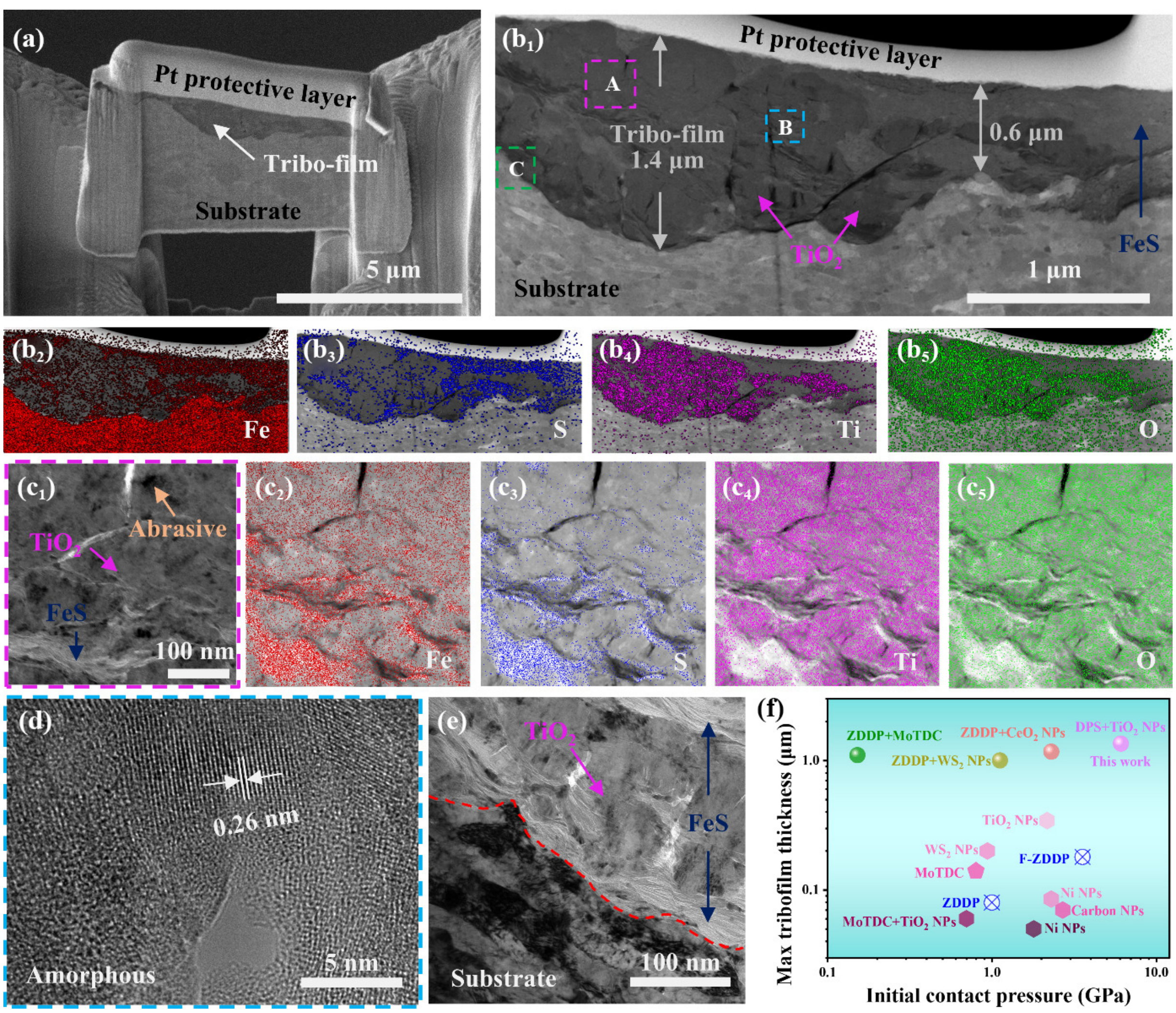

Fig. 5 Cross-sectional analysis of EP tribo-films on preweld balls lubricated with 400SN+DPS+TiO_2-OA (7,256 N, 10 s). (a) Cross-sectional SEM image of tribo-film. (b1–b5) and (c1–c5) Cross-sectional TEM images and EDS maps of tribo-films at different scales (c1–c5: a region in (b1)). (d) TEM image of contact area between tribo-film and steel ball substrate (B region in (b1)). (e) HRTEM image of tribo-film of C region in (b1). (f) Comparison of maximum tribo-film thickness in this work with that in other studies [22, 67–77].

3.5 Friction-reduction and AW performance of TiO_2-OA and DPS in 400SN

To clarify the interaction between DPS and TiO_2-OA, the reduction in friction and the AW performance of the lubricants were investigated using a four-ball tribometer and TE77. As shown in Fig. 6, 400SN+DPS exhibits the lowest average COF, while the WSD is analogous to that of 400SN. These results indicate that sulfated olefins exhibit inadequate AW performance, which is consistent with the findings of Zhang et al. [16]. This deficiency can be attributed to the insufficient adhesion and shear strength of the FeS tribo-film, rendering it prone to peeling and ultimately resulting in poor AW performance [78]. Figure 6 shows that the WSD and COF of 400SN+DPS+TiO_2-OA are 42% and 15% lower than those of 400SN, respectively. As illustrated in Fig. 6 and Fig. S9 in the ESM, the addition of free OA results in a reduction in the WSD of both 400SN and 400SN+DPS. Notably, the WSD of 400SN+DPS+TiO_2-OA is distinctly lower than those of 400SN+DPS and 400SN+DPS+OA (Fig. 6(b) and Fig. S9 in the ESM). Following the friction process, 400SN+DPS+TiO_2-OA maintains satisfactory dispersion stability (Fig. S9(c) in the ESM). These results suggest that TiO_2-OA effectively remedies the limitations of the FeS tribo-film. The TE77 friction results are similar to the four-ball friction results, demonstrating that the synergistic effect of DPS and TiO_2-OA NPs is beneficial for enhancing the friction-reduction and AW performance of 400SN base oil (Fig. S10 in the ESM). While the WSD of AW in Table S5 in the ESM is smaller than that of EP in Table S2 in the ESM, suggesting distinct lubrication mechanisms, the AW test relies on the boundary film for lubrication, whereas the EP test utilizes the EP film to prevent sintering. This difference is attributed to the rapid breakdown and significant wear of the boundary film during the EP process.

3.6 Surface characterization of AW wear scars

As illustrated in Fig. 7, the 3D profiles demonstrate that the wear surfaces of 400SN and 400SN + DPS are rather inhomogeneous, exhibiting distinct striped and concave areas. In contrast, the wear surfaces of the lubricant containing TiO_2-OAs are significantly flatter. The EDS maps show that the wear surfaces of both 400SN+DPS and 400SN+DPS+TiO_2-OA are enriched in

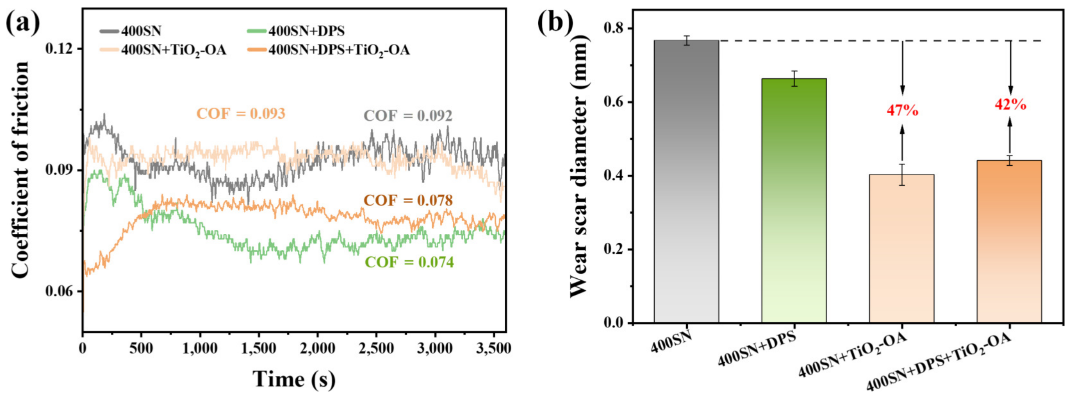

Fig. 6 Friction-reduction and AW tests under conditions of friction at 196 N, 1,200 r/min, and 75 °C for 60 min (3% DPS and 0.6% TiO_2-OA. (a) Real-time COF curve and (b) WSD.

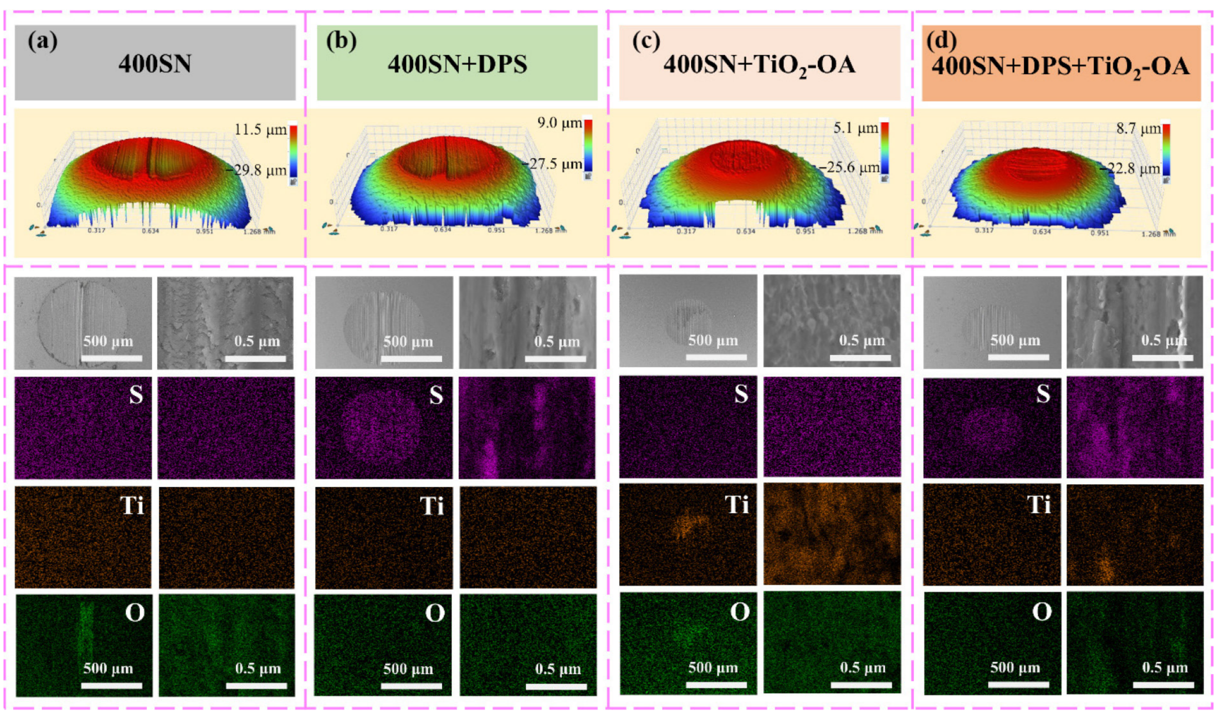

Fig. 7 3D profiles, SEM images, and EDS maps of AW wear scars (196 N, 1,200 r/min, and 75 °C for 60 min).

elemental S, whereas 400SN+DPS+TiO_2-OA is also enriched in elemental Ti. However, the lower Ti enrichment on the wear surface of 400SN+DPS+TiO_2-OA than on that of 400SN+TiO_2-OA is in line with our previous results, possibly due to the competing adsorption of sulfur-containing additives and TiO_2 NPs [32]. A comparison of the XPS spectra of the wear scars on AW (Fig. 8) and EP (Fig. 4) revealed a distinct difference, particularly in the S 2p spectra. This observation is in line with previous investigations, highlighting the oxidation of FeS to iron sulfate during the AW test due to extended operational periods and exposure to oxygen [6, 14, 16, 20, 32, 36, 37]. In contrast, iron sulfates were not evident in the relative EP test, suggesting differences in the chemical reactions and resulting products from interfacial friction between the AW and EP tests.

3.7 Formation mechanism of EP tribo-films

The synergistic effect of ZDDP in combination with NPs, including CeO_2, WS_2, SiO_2, TiO_2, Ti_3C_2, and NDs, has been demonstrated in several studies [22, 63, 71, 82–84]. These synergistic effects are widely attributed to NPs filling the tribo-film formed by ZDDP, which in turn produces a stronger nanocomposite tribo-film (i.e., a mechanically interlocked tribo-film). Furthermore, the majority of NPs remain in their initial chemical state within the tribo-film. Our findings are consistent with prior research indicating that TiO_2 filling of the matrix (FeS) formed by DPS enhances the mechanical properties of the tribo-film (Fig. 5 and Fig. S8 in the ESM). Although the synergistic effect of NPs with ZDDP was mainly observed in the AW test, which differs from the EP conditions, as shown in Fig. 5, the results in Fig. 6 also demonstrate a synergistic effect between TiO_2-OA NPs and DPS in the AW test. Importantly, the dispersion of NPs in the tribo-film generated under EP conditions may not be homogeneous, which is notably different from the state of dispersion observed in the AW test. Therefore, the synergistic effect of NPs with sulphur-containing additives can be attributed to the formation of mechanically interlocked tribo-films, in addition to effects related to tribo-chemical reactions.

On the basis of the analyses provided and our early investigations [31, 32], a mechanism for the synergistic enhancement of P_D values in 400SN by TiO_2-OA and DPS can be postulated. As depicted in Fig. 9, during the initial phase of friction, DPS and TiO_2-OA, which contain S–S and C=O groups, respectively, swiftly adhere and accumulate on the steel surface, creating an adsorbent film via S–Fe and O–Fe coordination bonds. This adsorption film initially functions as a lubricant upon the commencement of friction. With increasing load, the temperature increases, prompting the DPS to release more reactive sulphur, perpetuating the production of FeS films. Once the temperature exceeds 1,000 °C at the friction interface, the FeS film fails, leading to corrosion of the metal by the reactive sulphur. In the above process, the deposition of TiO_2-OA was coupled with the regeneration of FeS. TiO_2-OA helps form an EP tribo-film at the friction interface, increasing high-temperature resistance, strength, and micron-sized dimensions, thereby compensating for the wear resulting from the destruction of the FeS film due to high temperatures and extreme shear forces. Ultimately, a mechanically interlocked tribo-film is formed. Therefore, the key factors for optimizing the EP performance of lubricants are facilitating the rapid generation of FeS and the prompt aggregation, deposition, and enrichment of TiO_2 at the friction interface.

4 Conclusions

In conclusion, we conducted a comprehensive evaluation of the EP, friction reduction, and AW performance of TiO_2-OA NPs and DPS. The EP and AW wear scars were meticulously analyzed to explore the underlying mechanisms of the observed synergistic effects. The principal conclusions are summarized below.

(1) The synergistic effect of oil-soluble TiO_2-OA NPs and the sulfur-containing additive DPS improved the EP performance of DPS-containing lubricants by 29%.

(2) Analysis of AW and EP wear scars revealed notable differences in WSD, elemental distribution, and chemical state, indicating the presence of distinct synergistic mechanisms. Additionally, TiO_2-OA can be rapidly and effectively enriched at the friction interface, subsequently mitigating the wear generated by extreme shear forces.

(3) A cross-sectional analysis revealed that TiO_2 and FeS collectively formed a mechanically interlocked EP tribo-film with a maximum thickness of approximately 1.4 μm. The preferentially

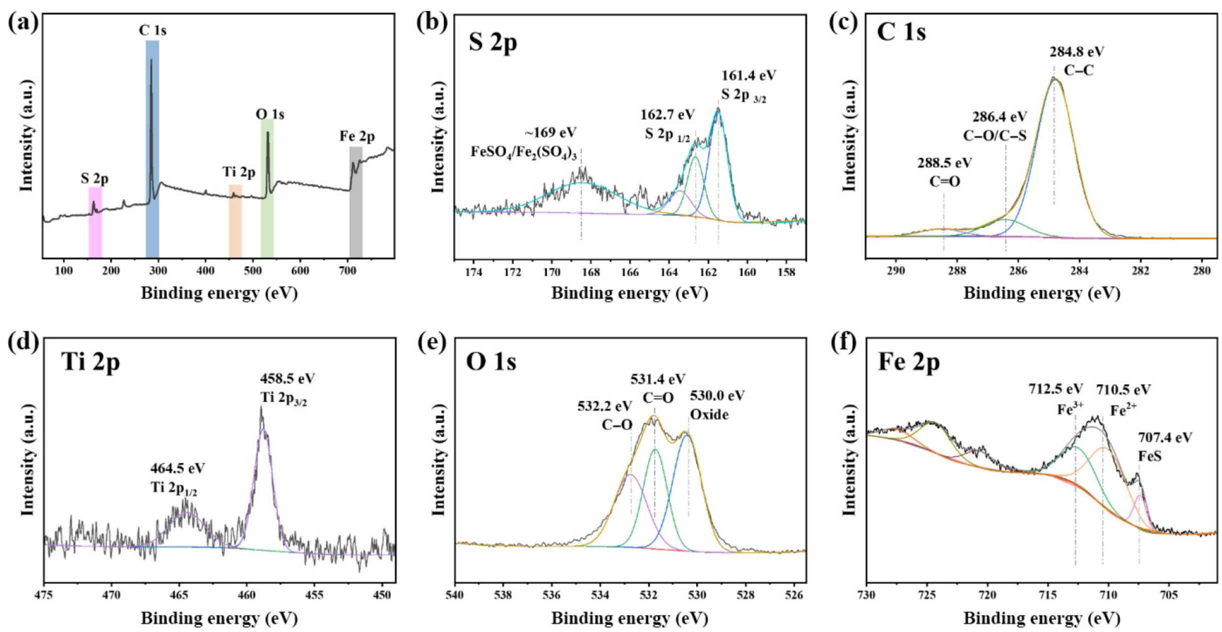

Fig. 8 XPS analysis of AW wear scar surface elements lubricated by 400SN+DPS+TiO_2-OA (196 N, 1,200 r/min, and 75 °C for 60 min).

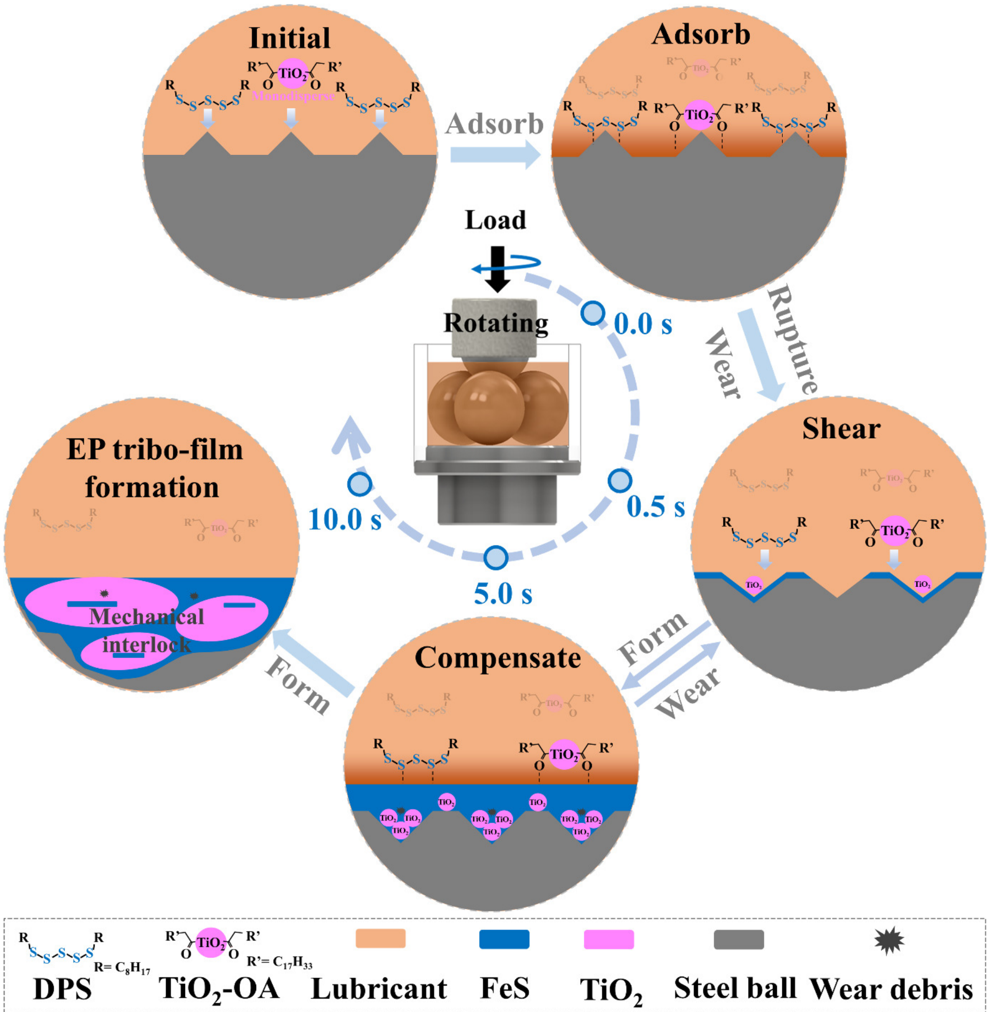

Fig. 9 Schematic diagram of synergistic mechanism of DPS and TiO_2-OA under EP conditions.

formed tribo-film was dominated by FeS, followed closely by a composite tribo-film consisting of aggregated TiO_2 and FeS as the friction time increased.

(4) The preferential formation of FeS and subsequent rapid enrichment and mechanical interlocking of TiO_2-OA NPs are both crucial for preventing welding and enhancing EP performance. This study provides novel perspectives and insights into the application and synergistic mechanism of NPs and sulfur-containing additives, which are expected to foster the broad application and development of NPs in the field of tribology.

Acknowledgements

This work was supported by the Shanghai Pujiang Program (No. 22PJ1414700), the International Partnership Program of the Chinese Academy of Sciences (No. 307GJHZ2022034GC), and the Key Project of the Henan Province Science and Technology Research and Development Joint Funds (No. 235101610007).

Declaration of competing interest

The authors have no competing interests to declare that are relevant to the content of this article.

Electronic Supplementary Material

Supplementary material is available in the online version of this article at https://doi.org/10.26599/FRICT.2025.9441098.

References

[1] Zhang Y, Chen H, Gao K, Li Y Z, Jiao J G, Xie G X, Luo J B. Macroscale superlubricity with high pressure enabled by partially oxidized violet phosphorus for engineering steel. *Adv Funct Mater* **34**(36): 2401143 (2024)

[2] Berman D, Erdemir A. Achieving ultralow friction and wear by tribocatalysis: Enabled by *In-operando* formation of nanocarbon films. *ACS Nano* **15**(12): 18865–18879 (2021)

[3] Holmberg K, Erdemir A. Influence of tribology on global energy consumption, costs and emissions. *Friction* **5**(3): 263–284 (2017)

[4] Özkan D, Sulukan E. Tribological behavior of the low-concentration boric acid and ZDDP lubricating oil mixtures. *Surf Interface Anal* **51**(8): 826–839 (2019)

[5] Qu J, Barnhill W C, Luo H M, Meyer H M III, Leonard D N, Landauer A K, Kheireddin B, Gao H, Papke B L, Dai S. Synergistic effects between phosphonium-alkylphosphate ionic liquids and zinc dialkyldithiophosphate (ZDDP) as lubricant additives. *Adv Mater* **27**(32): 4767–4774 (2015)

[6] Niu W X, Yuan M, Wang P F, Shi Q, Xu H, Dong J X. One-pot synthesis of SIB@ZIF-8 with enhanced anti-corrosion properties and excellent lubrication properties. *Tribol Int* **151**: 106491 (2020)

[7] Baş H S, Ali Beşirbeyoğlu M, Özen O. Investigation of tribological properties of MoS_2 and CaF_2 particles as oil additives and their effects on surface contact. *Lubr Sci* **36**(4): 314–329 (2024)

[8] Long R S, Yao Y, Zhang L E, Shang Q Y, Sun S N, Hu J S, Pape F, Marian M. Synergistic effects of graphene-added lubricants and

surface micro-texturing on the tribological behavior of thrust roller bearings. *Tribol Int* **198**: 109908 (2024)

[9] Holmberg K, Andersson P, Erdemir A. Global energy consumption due to friction in passenger cars. *Tribol Int* **47**: 221–234 (2012)

[10] Roache D C, Bumgardner C H, Zhang Y Y, Edwards D, DeGonia D, Rock B, Li X D. Chemo-mechanical characterization of phosphorus and sulfur containing ashless tribofilms on hypoid gear teeth. *Tribol Int* **158**: 106926 (2021)

[11] Bierla A, Fromentin G, Minfray C, Martin J M, Le Mogne T, Genet N. Mechanical and physico-chemical study of sulfur additives effect in milling of high strength steel. *Wear* **286**: 116–123 (2012)

[12] Khan T, Koide S, Tamura Y, Yamamoto H, Morina A, Neville A. Effects of using alternative extreme pressure (EP) and anti-wear (AW) additives with oxy-nitrided samples. *Tribol Lett* **66**: 43 (2018)

[13] Huang S Z, Wu Z B, Johannessen B, Long K C, Qing P, He P, Ji X B, Wei W F, Chen Y J, Chen L B. Interfacial friction enabling ≤ 20 μm thin free-standing lithium strips for lithium metal batteries. *Nat Commun* **14**: 5678 (2023)

[14] Li W M, Jiang C, Chao M R, Wang X B. Natural garlic oil as a high-performance, environmentally friendly, extreme pressure additive in lubricating oils. *ACS Sustain Chem Eng* **2**(4): 798–803 (2014)

[15] Gosvami N N, Bares J A, Mangolini F, Konicek A R, Yablon D G, Carpick R W. Mechanisms of antiwear tribofilm growth revealed *in situ* by single-asperity sliding contacts. *Science* **348**(6230): 102–106 (2015)

[16] Zhang R C, Xia Y, Zhang J C, Wang Y, Zhang H J, Hu X D, Xu X F. Effects of electrostatic catalysis on the formation of chemical reaction films with charged lubricant containing sulfurized isobutylene additive. *Tribol Int* **177**: 108012 (2023)

[17] Shen T J, Wang D X, Yun J, Liu Q L, Liu X H, Peng Z X. Tribological properties and tribochemical analysis of nano-cerium oxide and sulfurized isobutene in titanium complex grease. *Tribol Int* **93**: 332–346 (2016)

[18] Alves S M, Schroeter R B, dos Santos Bossardi J C, de Andrade C L F. Influence of EP additive on tool wear in drilling of compacted graphite iron. *J Braz Soc Mech Sci* **33**(2): 197–202 (2011)

[19] Lozinskii A V, Kuchin D P, Efimov V N, Pakhomova M I. Solving the problems of high-temperature sulfur corrosion in primary oil refineries. *Chem Tech Fuels Oil+* **57**(4): 613–618 (2021)

[20] Salinas Ruiz V R, Kuwahara T, Galipaud J, Masenelli-Varlot K, Ben Hassine M, Héau C, Stoll M, Mayrhofer L, Moras G, Martin J M, et al. Interplay of mechanics and chemistry governs wear of diamond-like carbon coatings interacting with ZDDP-additivated lubricants. *Nat Commun* **12**: 4550 (2021)

[21] Wright R A E, Wang K W, Qu J, Zhao B. Oil-soluble polymer brush grafted nanoparticles as effective lubricant additives for friction and wear reduction. *Angew Chem Int Edit* **55**(30): 8656–8660 (2016)

[22] Lei X, Zhang Y J, Zhang S M, Yang G B, Zhang C L, Zhang P Y. Study on the mechanism of rapid formation of ultra-thick tribofilm by CeO_2 nano additive and ZDDP. *Friction* **11**(1): 48–63 (2023)

[23] Rosenkranz A, Righi M C, Sumant A V, Anasori B, Mochalin V N. Perspectives of 2D MXene tribology. *Adv Mater* **35**(5): 2207757 (2023)

[24] Wyatt B C, Rosenkranz A, Anasori B. 2D MXenes: Tunable mechanical and tribological properties. *Adv Mater* **33**(17): 2007973 (2021)

[25] Xue S H, Cui Y H, Jin G K, Wang H Y, Liu S J, Ye Q, Wang H Q, Zhou F, Liu W M. Carbon dots with spatially-mediated-N/S-co-doping enabling one-year stable lubricant with oil leakage detection capability. *Small* **20**(29): 2312010 (2024)

[26] Maleki A, Vafaeenezhad H, Eslami-Farsani R. Polystyrene microcapsules containing linseed oil and SiC nanoparticles as a lubricant additive for boosting the self-healing and self-lubricating efficiency of epoxy coatings. *Tribol Int* **193**: 109428 (2024)

[27] Gao Y J, Sun R, Zhang, Xue Q J. Tribological properties of oleic acid: Modified TiO_2 nanoparticle in water. *Mat Sci Eng A—Struct* **286**(1): 149–151 (2000)

[28] Gao Y J, Chen G X, Oli Y, Zhang Z J, Xue Q J. Study on tribological properties of oleic acid-modified TiO_2 nanoparticle in water. *Wear* **252**(5–6): 454–458 (2002)

[29] Maurya U, Vasu V, Saini V. Nano-innovations in lubrication: Unveiling the synergistic boundary lubrication potential of zinc titanate with phosphonium ionic liquid. *Tribol Int* **199**: 109987 (2024)

[30] Guan J J, Ding Y P, Gao C, Xu Z Y, Xu X F, Wang Z L. Experimental study on turning performance of a novel nanofluid prepared by composites of MWCNTs. *Int J Adv Manuf Tech* **116**(7–8): 2373–2385 (2021)

[31] Zhang H, Han S, Hu W J, Li J S. Tribological study of TiO_2 nanoparticles modified with stearic acid as additives in lithium grease. *Ind Lubr Tribol* **73**(6): 904–910 (2021)

[32] Wang J B, Shen J W, Lu H Y, Hu W J, Li J S. Tuning the interfacial behavior of extreme pressure lubrication by stearic acid-modified TiO_2 nanoparticles. *Appl Surf Sci* **630**: 157510 (2023)

[33] Zhao X Y, Yang J Y, Tao D H, Xu X R. Tribological study of nitrogen plasma polymerized soybean oil with nitrogen heterocyclic structures. *Ind Crop Prod* **51**: 236–243 (2013)

[34] Zheng G L, Ding T M, Pang S H, Zheng L, Ren T H. Friction-condition-dependent sulfide and sulfate evolution on dialkylpentasulfide tribofilm studied by XANES. *Friction* **8**(5): 874–881 (2020)

[35] Najman M N, Kasrai M, Bancroft G M. X-ray absorption spectroscopy and atomic force microscopy of films generated from organosulfur extreme-pressure (EP) oil additives. *Tribol Lett* **14**(4): 225–235 (2003)

[36] Guan J J, Xu X F, Peng W. Tribological properties of phenolic resin bonded abrasive tools filled with two inclusion complexes of β-cyclodextrin and sulfur-containing additives. *P I Mech Eng J—J Eng* **228**(7): 725–734 (2014)

[37] Ma H X, Wu W, Wang Z Y. Bisurfactant-functionalized TiO_2 nanoparticles as additives of the lubricating oil. *Lubr Sci* **34**(7): 441–448 (2022)

[38] Roy J. The synthesis and applications of TiO_2 nanoparticles derived from phytochemical sources. *J Ind Eng Chem* **106**: 1–19 (2022)

[39] Erck R A, Song M, Li D S, Cosimbescu L. Investigations of polymethacrylate tribochemical films using X-ray spectroscopy and optical profilometry. *Tribol Lett* **69**: 26 (2021)

[40] Choudhury N D, Bhaumik S, Saha N, Kataki R. Investigating the tribological properties of TiO_2 nanoparticles added *Thevetia peruviana* and *Cucurbita pepo* L. blend oils. *Tribol Int* **197**: 109769 (2024)

[41] Wu H, Zhao J W, Xia W Z, Cheng X W, He A S, Yun J H, Wang L Z, Huang H, Jiao S H, Huang L, et al. A study of the tribological behaviour of TiO_2 nano-additive water-based lubricants. *Tribol Int* **109**: 398–408 (2017)

[42] Ranjan N, Shende R C, Kamaraj M, Ramaprabhu S. Utilization of TiO_2/gC_3N_4 nanoadditive to boost oxidative properties of vegetable oil for tribological application. *Friction* **9**(2): 273–287 (2021)

[43] Ong C L, Lai Y C, Tang W K, Heidelberg T, Khaligh N G, Juan J C. Tribological behavior of sulfonitrided tribofilm generated from non-corrosive dimercaptobenzothiadiazole-based additives as effective boundary lubrication layer. *J Mol Liq* **403**: 124751 (2024)

[44] Li J, Ma H B, Ren T H, Zhao Y D, Zheng L, Ma C Y, Han Y. The tribological chemistry of polysulfides in mineral oil and synthetic diester. *Appl Surf Sci* **254**(22): 7232–7236 (2008)

[45] Patil S, Rajurkar K, Patil S, Pratap A. Synthesis of guerbet esters and its application in drilling and grinding oil. *Tribol Int* **177**: 107993 (2023)

[46] US-ASTM. ASTM D4172-21 Standard test method for wear preventive characteristics of lubricating fluid (four-ball method). ASTM, 2021.

[47] US-ASTM. ASTM D2783-21 Standard test method for measurement of extreme-pressure properties of lubricating fluids (four-ball method). ASTM, 2021.

[48] Zhang H W, Bao L, Zhou Q W, Song G. Facilitate nitrogen fixation photoreaction over decorated composited dots on the (001) facet

exposed anatase titanium dioxide nanosheets. *J Environ Chem Eng* **12**(5): 114034 (2024)
[49] Cai J Y, Yu D B, Zhang Y, Yao S Z, Zhang X R, Cui J W, Wang Y, Liu J Q, Yu C P, Sun X C, et al. A facile synthesis of porous amorphous/crystalline TiO_2 hybrids for enhanced electrochromic performances. *J Electroanal Chem* **914**: 116304 (2022)
[50] Pal M, Serrano J G, Santiago P, Pal U. Size-controlled synthesis of spherical TiO_2 nanoparticles: Morphology, crystallization, and phase transition. *J Phys Chem C* **111**(1): 96–102 (2007)
[51] Jia T, Zhang J, Wu J, Wang D L, Liu Q Z, Qi Y F, Hu B, He P, Pan W G, Qi X M. Synthesis amorphous TiO_2 with oxygen vacancy as carriers transport channels for enhancing photocatalytic activity. *Mater Lett* **265**: 127465 (2020)
[52] Chakraborty S, Panigrahi P K. Stability of nanofluid: A review. *Appl Therm Eng* **174**: 115259 (2020)
[53] Wang J, Yang X, Klemeš J J, Tian K, Ma T, Sunden B. A review on nanofluid stability: Preparation and application. *Renew Sust Energ Rev* **188**: 113854 (2023)
[54] Shi Q, Chen Z F, Song Z W, Li J P, Dong J X. Synthesis of ZIF-8 and ZIF-67 by steam-assisted conversion and an investigation of their tribological behaviors. *Angew Chem Int Edit* **50**(3): 672–675 (2011)
[55] An F P, Liu Q L, Zhang H, Fan J W, Zhang Y L, Li Y S, Wang G C, Wu J, Chong X Y. Stability, electronic structure, mechanical properties and lattice thermal conductivity of FeS and FeS_2 polymorphs. *Mod Phys Lett B* **35**(13): 2150225 (2021)
[56] Bonkerud J, Zimmermann C, Weiser P M, Vines L, Monakhov E V. On the permittivity of titanium dioxide. *Sci Rep* **11**: 12443 (2021)
[57] Wu Y Y, Tsui W C, Liu T C. Experimental analysis of tribological properties of lubricating oils with nanoparticle additives. *Wear* **262**(7–8): 819–825 (2007)
[58] Low J, Dai B Z, Tong T, Jiang C J, Yu J G. *In situ* irradiated X-ray photoelectron spectroscopy investigation on a direct Z-scheme TiO_2/CdS composite film photocatalyst. *Adv Mater* **31**(5): 1807920 (2019)
[59] Cui Y H, Xue S H, Wang T T, Liu S J, Ye Q, Zhou F, Liu W M. Core-rim structured MXene@SiO_2 composites as oil-based additives for enhanced tribological properties. *Friction* **12**(8): 1728–1740 (2024)
[60] Xu W Y, Yang G B, Zhang S M, Xu J, Zhang Y J, Sun T H, Song N N, Yu L G, Zhang P Y. Tribological properties and tribomechanism of nickel nanoparticles *in-situ* synthesized in rapeseed oil. *Friction* **12**(3): 474–489 (2024)
[61] Wen P, Lei Y Z, Yan Q Q, Han Y Y, Fan M J. Multilayer tribofilm: An unique structure to strengthen interface tribological behaviors. *ACS Appl Mater Inter* **13**(9): 11524–11534 (2021)
[62] Yamashita N, Hirayama T. Effect of atmospheric gas on ZDDP tribofilm formation. *Tribol Int* **193**: 109400 (2024)
[63] Piya A K, Yang L, Al Sheikh Omar A, Emami N, Morina A. Synergistic lubrication mechanism of nanodiamonds with organic friction modifier. *Carbon* **218**: 118742 (2024)
[64] Shangguan E B, Guo L T, Li F, Wang Q, Li J, Li Q M, Chang Z R, Yuan X Z. FeS anchored reduced graphene oxide nanosheets as advanced anode material with superior high-rate performance for alkaline secondary batteries. *J Power Sources* **327**: 187–195 (2016)
[65] Liu H L, Lv C X, Chen S, Song X Y, Liu B H, Sun J, Zhang H W, Yang D J, She X L, Zhao X L. Fe-alginate biomass-derived FeS/3D interconnected carbon nanofiber aerogels as anodes for high performance sodium-ion batteries. *J Alloy Compd* **795**: 54–59 (2019)
[66] Wei X, Li W H, Shi J A, Gu L, Yu Y. FeS@C on carbon cloth as flexible electrode for both lithium and sodium storage. *ACS Appl Mater Inter* **7**(50): 27804–27809 (2015)
[67] Ueda M, Kadiric A, Spikes H. Influence of steel surface composition on ZDDP tribofilm growth using ion implantation. *Tribol Lett* **69**(2): 62 (2021)
[68] Li Y R, Pereira G, Kasrai M, Norton P R. The effect of steel hardness on the performance of ZDDP antiwear films: A multi-technique approach. *Tribol Lett* **29**(3): 201–211 (2008)
[69] Mourhatch R, Aswath P B. Tribological behavior and nature of tribofilms generated from fluorinated ZDDP in comparison to ZDDP under extreme pressure conditions: Part II: Morphology and nanoscale properties of tribofilms. *Tribol Int* **44**(3): 201–210 (2011)
[70] De Feo M, Minfray C, De Barros Bouchet M I, Thiebaut B, Le Mogne T, Vacher B, Martin J M. Ageing impact on tribological properties of MoDTC-containing base oil. *Tribol Int* **92**: 126–135 (2015)
[71] Aldana P U, Dassenoy F, Vacher B, Le Mogne T, Thiebaut B. WS_2 nanoparticles anti-wear and friction reducing properties on rough surfaces in the presence of ZDDP additive. *Tribol Int* **102**: 213–221 (2016)
[72] Ratoi M, Niste V B, Walker J, Zekonyte J. Mechanism of action of WS_2 lubricant nanoadditives in high-pressure contacts. *Tribol Lett* **52**(1): 81–91 (2013)
[73] Hu J S, Zhang Y J, Yang G B, Gao C P, Song N N, Zhang S M, Zhang P Y. *In-situ* formed carbon based composite tribo-film with ultra-high load bearing capacity. *Tribol Int* **152**: 106577 (2020)
[74] Hong F T, Schneider A, Sarathy S M. Enhanced lubrication by core–shell TiO_2 nanoparticles modified with gallic acid ester. *Tribol Int* **146**: 106263 (2020)
[75] Deshpande P, Dassenoy F, Minfray C, Jenei I Z, Le Mogne T, Thiebaut B. Effect of adding TiO_2 nanoparticles to a lubricant containing MoDTC on the tribological behavior of steel/steel contacts under boundary lubrication conditions. *Tribol Lett* **68**: 39 (2020)
[76] Wang Y X, Liu S, Cui Y H, Bai W, Liu S J, Ye Q, Zhou F, Liu W M. *In-situ* pyrolysis synthesis of multi-element (F, N, S) co-doped porous carbon nanospheres as lubricating additives with improved tribological behaviors. *Carbon* **218**: 118724 (2024)
[77] Jiménez A E, Morina A, Neville A, Bermúdez M D. Surface interactions and tribochemistry in boundary lubrication of hypereutectic aluminium: Silicon alloys. *P I Mech Eng J—J Eng* **223**(3): 593–601 (2009)
[78] Zheng G L, Ding T M, Zheng L, Ren T H. The lubrication effectiveness of dialkylpentasulfide in synthetic ester and its emulsion. *Tribol Int* **122**: 76–83 (2018)
[79] Fei Y W, Bertka C M, Finger L W. High-pressure iron-sulfur compound, Fe_3S_2, and melting relations in the Fe–FeS system. *Science* **275**(5306): 1621–1623 (1997)
[80] Li H G, Zhang Y B, Li C H, Zhou Z M, Nie X L, Chen Y, Cao H J, Liu B, Zhang N Q, Said Z, et al. Extreme pressure and antiwear additives for lubricant: Academic insights and perspectives. *Int J Adv Manuf Tech* **120**(1–2): 8614 (2022)
[81] Hsu C Y, Mahmoud Z H, Abdullaev S, Ali F K, Ali Naeem Y, Mzahim Mizher R, Morad Karim M, Abdulwahid A S, Ahmadi Z, Habibzadeh S, et al. Nano titanium oxide (nano-TiO_2): A review of synthesis methods, properties, and applications. *Case Stud Chem Environ Eng* **9**: 100626 (2024)
[82] Syed J, Hakkim N L, Nebhani L, Gosvami N N. Enhancing tribological properties of lubricated contacts via synergistic interactions of green silica nanoparticles and ZDDP. *Tribol Int* **197**: 109829 (2024)
[83] Sharma V, Timmons R B, Erdemir A, Aswath P B. Synergistic and antagonistic interaction between ZDDP and TiO_2 nanoparticles under boundary lubrication. *Tribol Int* **202**: 110299 (2025)
[84] Liu H C, Wang X Y, Zhao L H, Yang S Y, Zhang X. Synergistic tribological effects of $Ti_3C_2T_x$ MXene and ZDDP under simple grafting strategies for efficient lubrication. *ACS Appl Mater Inter* **16**(43): 59096–59108 (2024)

Kai Zeng obtained his bachelor degree from Hainan University in 2016, followed by a master degree from Wuhan University of Technology. He is currently pursuing his doctoral degree at the Shanghai Advanced Research Institute, Chinese Academy of Sciences. His research interests include the synthesis and functionalization of nanomaterials, as well as the study of their tribological mechanisms.

Wenjing Hu received her Ph.D. degree from the University of Chinese Academy of Sciences. As a senior engineer at the Shanghai Advanced Research Institute, Chinese Academy of Sciences, she specializes in the design, synthesis, conformational relationship, and mechanism of lubricant additives.

Jiusheng Li received his Ph.D. degree from Shanghai Jiaotong University in 2002 and worked at the PetroChina Lanzhou Lubricant R&D Center for 10 years after graduation. Since 2012, he has been working as a professor at the Shanghai Advanced Research Institute, Chinese Academy of Sciences. His research interests include the design, synthesis, and investigation of the friction mechanisms of synthetic base oils and high-performance additives.